Shell model and band structures in O-19

von Oertzen, W; Milin, M; Dorsch, T; Bohlen, HG; Kruecken, R; Faestermann, T; Hertenberger, R; Mahgoub, M; Wheldon, Carl; Wirth, HF; Kokalova, Tz

DOI:
10.1140/epja/i2010-11060-7

Document Version
Publisher's PDF, also known as Version of record

Citation for published version (Harvard):
von Oertzen, W, Milin, M, Dorsch, T, Bohlen, HG, Kruecken, R, Faestermann, T, Hertenberger, R, Mahgoub, M, Wheldon, C, Wirth, HF & Kokalova, T 2010, 'Shell model and band structures in O-19', *European Physical Journal A*, vol. 46, no. 3, pp. 345-358. https://doi.org/10.1140/epja/i2010-11060-7

EPJ A
Hadrons and Nuclei

EPJ.org
your physics journal

Eur. Phys. J. A **46**, 345–358 (2010) DOI: 10.1140/epja/i2010-11060-7

Shell model and band structures in ^{19}O

W. von Oertzen, M. Milin, T. Dorsch, H.G. Bohlen, R. Krücken, T. Faestermann, R. Hertenberger, Tz. Kokalova, M. Mahgoub, C. Wheldon and H.-F. Wirth

EDP SCIENCES
Società Italiana di Fisica
Springer

Eur. Phys. J. A **46**, 345–358 (2010)
DOI 10.1140/epja/i2010-11060-7

THE EUROPEAN PHYSICAL JOURNAL A

Regular Article – Experimental Physics

Shell model and band structures in ^{19}O

W. von Oertzen[1,a], M. Milin[2,b], T. Dorsch[1,3], H.G. Bohlen[1], R. Krücken[3], T. Faestermann[3], R. Hertenberger[4], Tz. Kokalova[1,c], M. Mahgoub[3], C. Wheldon[1,c], and H.-F. Wirth[3,4]

[1] Helmholtz-Zentrum Berlin, Hahn-Meitner Platz 1, D-14109 Berlin, Germany
[2] Department of Physics, Faculty of Science, University of Zagreb, Bijenička 32, HR-10000 Zagreb, Croatia
[3] Technische Universität München, James Frankstr. 1, D-85748 Garching, Germany
[4] Sektion Physik der Universität München, Am Coulombwall 1, D-85748 Garching, Germany

Received: 30 August 2010 / Revised: 18 October 2010
Published online: 19 November 2010 –
Communicated by N. Alamanos

Abstract. We have studied the reaction (^{7}Li, p) on ^{13}C targets at E_{lab} = 44 MeV, populating states in the oxygen isotope ^{19}O. The experiments were performed at the Tandem Laboratory (Maier-Leibniz Laboratorium) using the high-resolution Q3D magnetic spectrometer. States were populated up to an excitation energy of 21 MeV, with an overall energy resolution of 45 keV. We discuss shell model states and cluster bands related to the rotational bands in the ^{18}O-isotope, using the weak-coupling approach. Similar to ^{18}O, the broken intrinsic reflection symmetry in these states must give rise to rotational bands as parity doublets, so two $K = 3/2$ bands (parities, + and −) are proposed with large moments of inertia. These are discussed in terms of an underlying cluster structure, (^{14}C ⊗ n ⊗ α). An extended molecular binding diagram is proposed which includes the ^{14}C-cluster.

1 Introduction

Clustering and deformations are observed as general phenomena in light nuclei at excitation energies close to the alpha and other cluster decay thresholds [1–4]. For oxygen isotopes, such structures have recently been seen in ^{17}O [5] and established for ^{18}O [6] and ^{20}O [7,8]. Compared to the $N = Z$ case, the additional neutrons yield molecular structures with binding effects based on covalent molecular neutron orbitals. In a weak-coupling picture such states in ^{19}O can be based on the now known band structure in ^{18}O and ^{20}O. While early studies were based on the "Ikeda" diagram for $N = Z$ nuclei [1], for the nuclei with extra neutrons an extended diagram should be used, as proposed by von Oertzen [4]. In the former scheme α-clusters and ^{16}O-clusters are the main ingredients, while with the recent study of ^{18}O [6] it was concluded that the ^{14}C nucleus has to be added to the extended diagram (see sect. 6 and fig. 3), because it has equivalent cluster properties as ^{16}O. These specific properties of ^{14}C are: i) closed p-shell, even better closure than in ^{16}O —this results in a perfect spherical shape; ii) the first excited states at ≈ 6 MeV of excitation; iii) the very high binding energies of nucleons: $E_B(p) = 20.83$ MeV, $E_B(n) = 8.17$ MeV; iv) similarly high binding energy for α-particles: $E_B(\alpha) = 12.02$ MeV. Therefore, we expect pronounced clustering and molecular configurations in all the oxygen isotopes [8] with neutron excess, ^{18,19,20}O. These would be very similar in structure to the ^{20,21,22}Ne isotopes which are built on a configuration having ^{16}O instead of ^{14}C as the larger cluster (see also ref. [9]). The overview of possible structures is given in fig. 1, where the shell model and cluster model configurations are illustrated in a schematic way.

So far, we have almost no knowledge on the states with α-cluster structure in ^{19}O. A few experimental studies [10] can be considered as the direct investigation of the α-cluster properties of the ^{19}O nucleus, expected close to the α-decay threshold. For example, the total cross-sections for the α_0 and α_1 groups in the ^{18}O$(n,\alpha)^{15}$C reaction have been measured for E_n = 7.5 to 8.6 MeV [11]; resonances have been reported at $E_x = 11.25$ and 11.58 MeV, and these are also the highest states listed in the last compilation [10] of the ^{19}O states. Fortune *et al.* [12] studied the low-lying levels of ^{19}O with the (^{7}Li, p) reaction at a beam energy of 20.4 MeV, at this energy the reaction mechanism is shown to be mainly a compound nuclear reaction, with contributions from a direct transfer mechanism for higher-lying states of high spin.

From the shell model point of view, the ^{19}O nucleus was usually described considering three neutrons outside of an ^{16}O core (a reasonably good closed-shell nucleus), but calculations with Pauli-allowed *pds* configurations

[a] e-mail: oertzen@helmholtz-berlin.de
[b] e-mail: matko.milin@phy.hr
[c] *Present address:* School of Physics and Astronomy, University of Birmingham, Edgbaston, B15 2TT, Birmingham, UK.

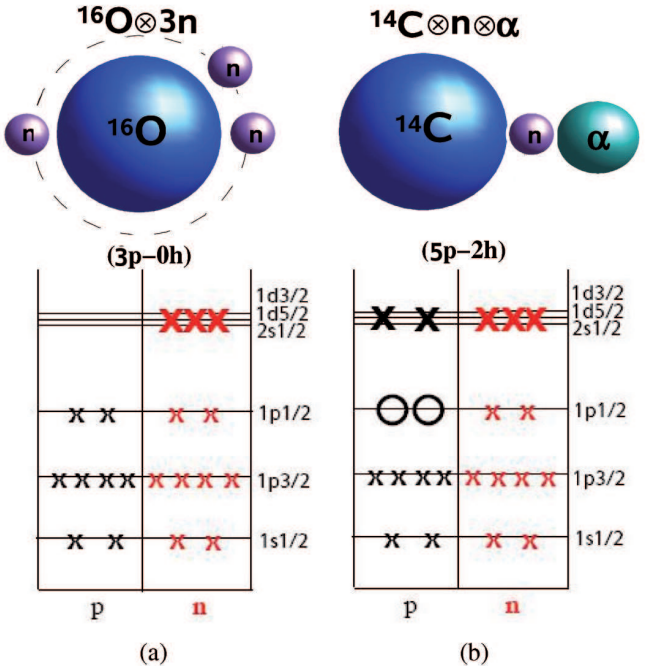

Fig. 1. (Color online) Cluster and shell model structure of states in ^{19}O. The cluster structure can be described in the shell model by multi-particle–multi-hole excitations (5p-2h) for positive parities. For negative parities the parity doublet partner, a (4p-2h)⊗(n, f-shell) excitation, is difficult to create in the shell (Nilsson) model, they must be considered in the cluster model.

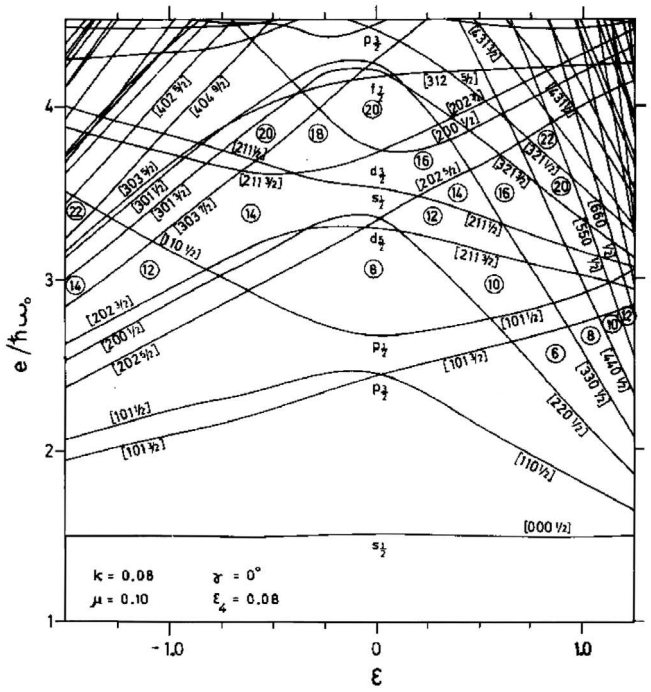

Fig. 2. The Nilsson model for neutron orbits in the p-, sd- and f-shells (for ^{19}O). We expect the population of the $d_{5/2}$, $K = 1/2, 3/2$ orbits for prolate deformation.

outside an inert ^{12}C core were also performed [13]. Detailed full shell model calculation for ^{19}O using a modification of the Millener-Kurath interaction has been performed by Warburton [14]. A more recent detailed study of the level structure (low-spin values) of ^{19}O was obtained from β-delayed neutron emission measurements [15]; γ-decays between states of ^{19}O were also observed and detailed shell model calculations given. Continuum shell model calculations were also performed [16,17] for all oxygen isotopes; low-lying states were also discussed within the simple shell model in ref. [18]. It is interesting to note that multi-particle–multi-hole configurations in the wave functions of low-lying ^{18,19}O states were shown to be essential for the understanding the ^{18}O$(n,\gamma)^{19}$O reaction at low energies [19,20].

Shell model calculations for ^{19}O have also been recently performed in ref. [21] with the OXBASH code [22] and within the "*psdpn*" model space; detailed comparison between the shell model configurations in ^{17}C and ^{19}O have also been given in that work (such comparison have previously been shown to be very useful for the discussion of ^{16}C / ^{18}O shell model states [23]). Shell model calculations with the OXBASH code were also given in ref. [24]; several states of the 5p-2h character were identified at low excitation energies (see sect. 5).

Low-lying positive-parity states in ^{19}O were also studied with the generator coordinate method [25], giving an overall excellent agreement with experimental data up to $E_x = 3$ MeV. The recent AMD (antisymmetrised molecular dynamics) calculations by Furutachi *et al.* [26,27] for the isotopes ^{18,20}O form also a useful quantitative basis for the comparison with the present measurements for ^{19}O.

In earlier work on configurations in the neighbouring nucleus ^{18}O (which has many states with similar cluster structure) emphasis was put on states with the intrinsic (^{14}C ⊗ α)-structure with dipole and octupole moments, and expectation of the $E1$ γ-transitions [28,29]. We expect low-lying $E1$ γ-transitions also in ^{19}O between members of rotational bands, which belong to parity doublets. The intrinsic quadrupole and octupole deformations have been discussed recently by Sato *et al.* [30]. We can look into the Nilsson diagram in fig. 2 in order to place the valence neutrons in the Nilsson orbits. We observe that two neutrons are in the lowest $K = 1/2$ orbit for the deformed shell model in ^{18}O and the last neutron is in the $K = 3/2$ orbit. The third neutron with $K = 3/2$ is coupled to the rotational bands in ^{18}O (see sect. 4). We expect therefore rotational bands, parallel to those in ^{18}O (because moments of inertia are similar), with $K = 3/2$ and a parity inversion doublet (parities + and −).

In the shell model framework deformations and rotational bands appear as multi-particle–multi-hole excitations (xp-yh). The positive-parity band is easily described similar to the particle-hole structure in ^{18}O. The corresponding negative-parity states are generally difficult to obtain in the shell model. In the cluster model the negative-parity bands appear as a consequence of the intrinsic reflection asymmetry of the cluster configurations. In ^{18}O these are excited bands, two bands with quantum

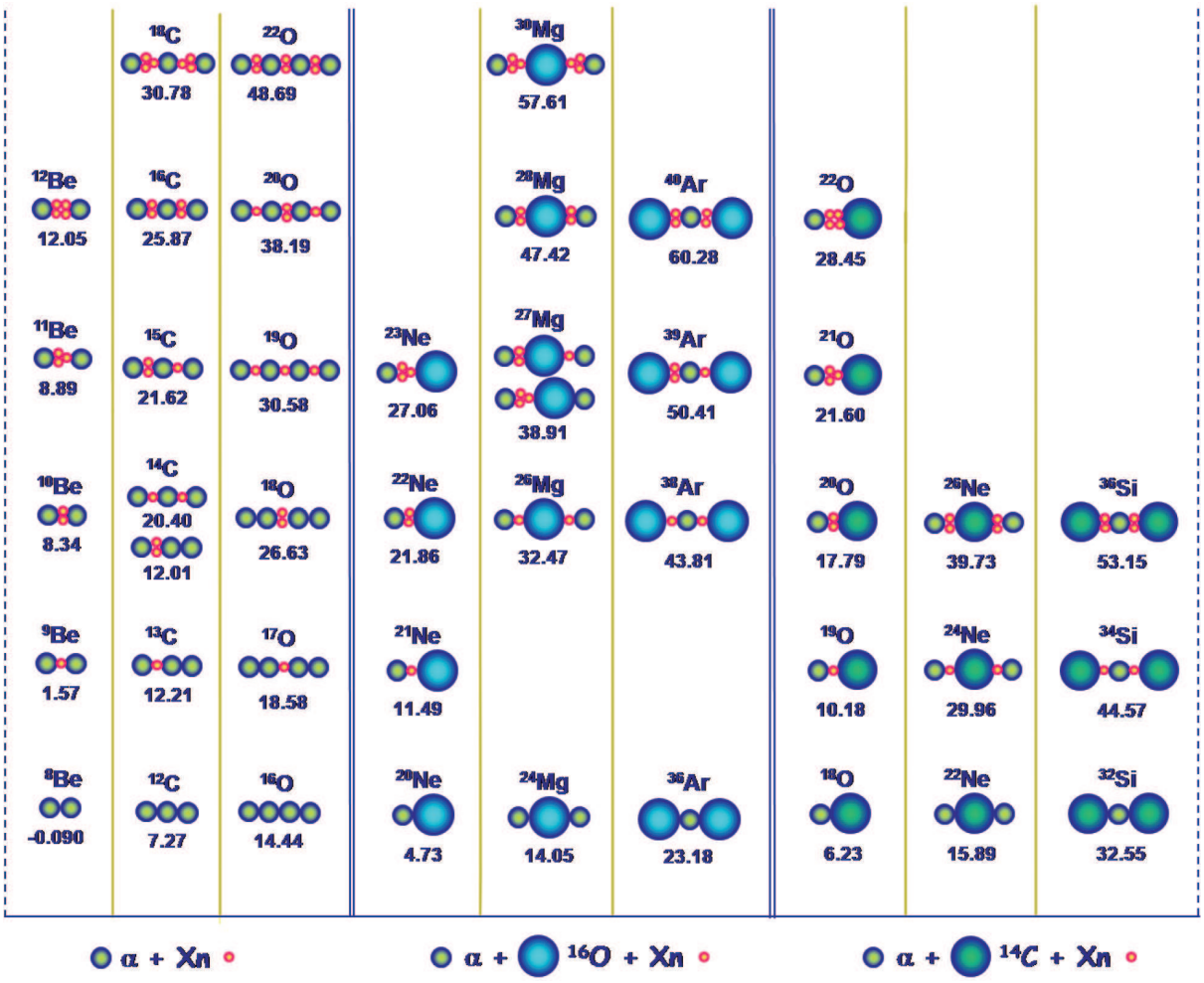

Fig. 3. (Color online) "Extended Ikeda Diagram": schematic overview of covalent molecular structures with valence neutrons in light $N > Z$ nuclei, with α-particles, ^{16}O- and ^{14}C-clusters. Threshold energies (in MeV) are given for the relevant decompositions.

numbers $K = 0_2^+$ and $K = 0_2^-$, the corresponding structures are (4p-2h, 5p-3h). Similarly, we expect an inversion doublet in ^{19}O for the cluster states. The molecular orbitals for the extra valence neutron would be analogous to the ^{21}Ne case [4] with the $(^{16}\mathrm{O}\otimes n\otimes\alpha)$ configuration. Such covalent neutron configurations are also predicted for even number of neutrons in the AMD calculations by Furutachi and Kanada-Enyo [27] for ^{18,20}O. Quite important for the present work are results for ^{18}O with the same reaction [6] on ^{12}C —the AMD calculations are also cited there and the effect of mixing of cluster and shell structure is found to be important for the states at lower excitation energy.

As in the work on ^{18}O, the multi-nucleon "transfer" reaction $(^7\mathrm{Li}, p)$ on ^{13}C has been used, which can populate both shell model states in ^{19}O as well as those with cluster structure. The reaction has similar properties as the multi-nucleon transfer reaction, $(^7\mathrm{Li}, d)$, which has been successfully used to study the cluster states in ^{14}C [31]. Due to the large angular-momentum mismatch between the incoming and outgoing channels in the $^{13}\mathrm{C}(^7\mathrm{Li}, p)$ reaction (between ^{7}Li and p to be specific), the reaction is expected to populate strongly yrast states of higher spin. This is true independent of the reaction mechanism. Also independent of the reaction mechanism, we expect within the same rotational band a dependence of the cross-section on $(2J+1)$, the spin multiplicity, with some variations due to the varying matching conditions as a function of spin. Contributions from a direct reaction are also expected at this energy. This feature, as well as the energy systematics (dependence of the energy on $J(J+1)$) and the expected close correspondence to the rotational bands observed in ^{18}O, are used to establish preliminary spin assignments for rotational bands in ^{19}O.

With the results on ^{19}O and ^{18}O we may further conclude that the strongly bound ^{14}C nucleus has equivalent properties as a cluster as ^{16}O. It is interesting to note that, although ^{14}C and ^{16}O are almost perfect spheres in their ground states, already their first excited states at ≈ 6 MeV show rather pronounced deformation due to clustering [31,32]. The similarity between ^{14}C and ^{16}O and the present results on oxygen isotopes suggest that the extended Ikeda diagram [4] with valence neutrons in covalent orbits must be revised to include the ^{14}C-cluster; this is shown in fig. 3.

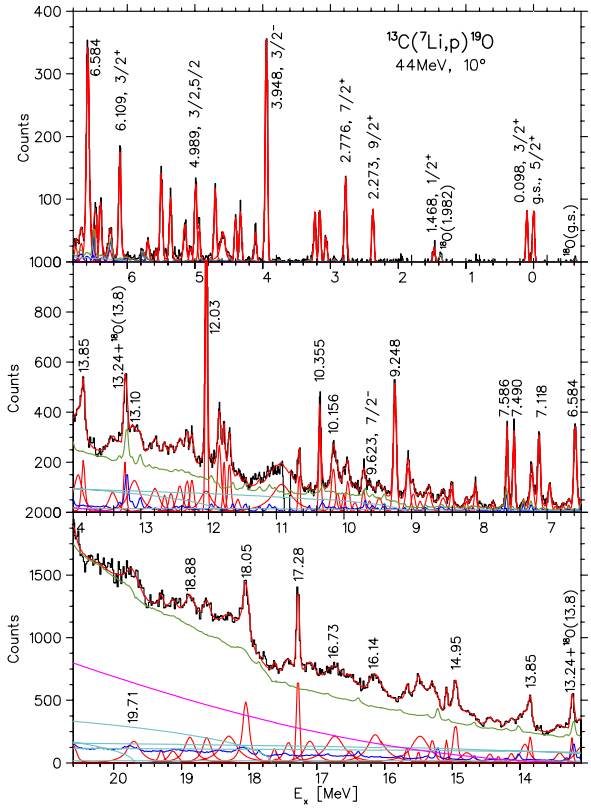

Fig. 4. (Color online) Energy spectrum of protons obtained with the Q3D-spectrometer for the reaction ^{7}Li+^{13}C $\rightarrow p+^{19}$O measured at 44.0 MeV incident energy and $\theta_{lab} = 10°$.

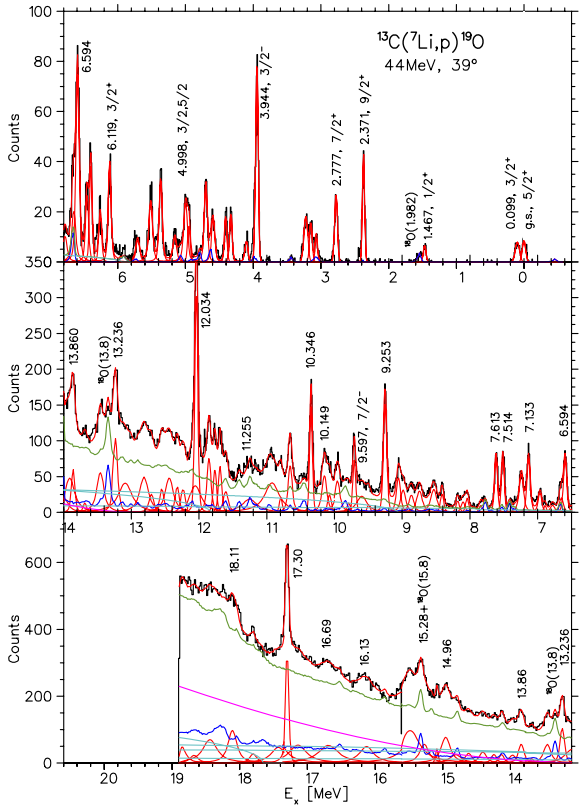

Fig. 5. (Color online) As fig. 4, energy spectrum of protons obtained with the Q3D-spectrometer for the reaction ^{7}Li + ^{13}C $\rightarrow p+^{19}$O at $\theta_{lab} = 39°$. The calculation of the continuous backgrounds is explained in the main text.

2 Experimental set-up and results

The experiments have been performed at the Tandem-van-de-Graaf accelerator of the Maier-Leibniz Laboratorium (MLL) at the Technical University and the Ludwig-Maximilians-University in Munich. The incident energy of ^{7}Li was 44 MeV, which allowed the population of states with excitation energies up to 21 MeV. The ^{7}Li$^{(3+)}$-beam intensity was typically about 200 nA. The (^{7}Li, p)-reaction has been measured at the Q3D magnetic spectrometer and the outgoing protons were identified by the focal plane detector using the energy loss in a gas-filled chamber and the light output of a scintillator behind it. The position in the focal plane was established using the delay-line read-out technique. Further details of the detector in the focal plane and the experimental set-up are given in refs. [6,8]. The ^{13}C targets consisted of 100 μg/cm^2 with an enrichment of 96.4%. For the potential contributions from oxygen a V_2O_5 target on an ^{12}C backing of 20 μg/cm^2 was used. Only small contributions from oxygen ($< 1.6\%$) and from ^{12}C (2.0%) were observed in the proton spectra.

The experimental procedure has been described in detail in refs. [6,8]. The measurements have been performed at three scattering angles: $\theta_{lab} = 10°$, 20° and 39°. The solid angle was 13.85 msr (horizontal width: 6° and vertical width: 7°). Ten (10) field settings (with regions of overlap of 15%) were needed per angle in order to cover an excitation energy range of 21 MeV. The resulting ten parts of the spectra were normalised and joined together in the overlapping regions, the counting rates were adjusted to a common scale. The resolution becomes worse at the larger angles due to larger values of the kinematic factor, which influences the final width due to a limiting value of the beam emittance. The proton spectra at $\theta_{lab} = 10°$ and 39° are shown in fig. 4 and fig. 5. Strong and rather narrow lines are observed well above the particle thresholds for α and neutron emission at 8.96 MeV and 3.96 MeV, respectively. The particle thresholds for ^{19}O are listed in table 1.

Table 1. Particle thresholds for ^{19}O.

S_α [MeV]	S_n [MeV]	S_{2n} [MeV]	S_p [MeV]
8.96	3.96	12.00	17.94

The spectra have been fitted for the lines with Gaussians, and above particle thresholds with Breit-Wigner line shapes, their intrinsic width has been obtained using the fitting code SPEC [33]. The larger number of narrow states at higher excitation energy points to their high spins and potentially to cluster structure. The energy calibration was obtained with the positions of the sharp well-known levels [10] in ^{19}O below 10 MeV, the overall agreement up to 11 MeV excitation energy was found to be

within 5 keV. In this analysis 109 states were identified, with more than 50 of them new.

The spectra contain some experimental background due to target contaminants mainly ^{12}C, these are marked as ^{18}O in the spectra, and were obtained experimentally with the same spectrometer settings. At higher excitation energies a three- and four-body continuum appears, starting at the corresponding thresholds. The flat backgrounds in figs. 4 and 5 correspond to the 3-body (and 4-body) phase-space distribution (blue lines) for three particles, n and ^{18}O (both not detected) and p (detected), p and ^{18}N* (both not detected). At about 12.8 MeV the 4-body phase-space distribution ($p+n+n+^{16}$O) (pink line) becomes visible, and a correct description of this background is quite important for the final fit. Actually the cited uncertainties in the yields of states at higher excitation energy partially are due to the determinations of the 3-4-body background. It was calculated using the code SPEC [33] as described in ref. [6]. The green line in fig. 4 is the sum of all phase-space distributions. Such spectra also exist at 20° and 39°, the latter is shown in fig. 5. The spectra are obtained by combining 10 magnetic-field settings, in the overlap regions of the individual spectra some states have problems with counting rates due to decreasing detection efficiency causing sometimes some systematic error in the yields. However, with the other angles these overlaps usually occur at different regions of excitation energies, so these errors can be cleared and understood. Nevertheless there are a few cases where the systematics of the cross-sections has to be considered with care by inspecting the relevant regions in the spectra of figs. 4 and 5.

3 Shell model and cluster structure

Among the light *sd*-shell nuclei, the structure of ^{19}O is expected to have one of the simplest interpretations within the shell model. For most of the low-lying positive-parity states, it is convenient to think of this nucleus as having three neutrons outside of an ^{16}O core —the structure of many of the low-lying states is then dominated by the $(sd)^3$ configurations. Detailed shell model calculations are given in ref. [14].

From the cluster model point of view, the different structures of the ^{19}O nucleus will be characterised by configurations very similar to ^{18}O (see fig. 1) as: i) ($^{16}\mathrm{O}\otimes 3n$), or as ii) ($^{14}\mathrm{C}\otimes 1n\otimes\alpha$), and iii) ($^{12}\mathrm{C}\otimes 3n\otimes\alpha$). All these structures can be populated in the $^{13}\mathrm{C}(^7\mathrm{Li},p)^{19}\mathrm{O}$ reaction. In this case we transfer "^{6}He" or rather an α-particle and 2 neutrons to the ^{13}C target in an arbitrary sequence. The configuration i), the $^{16}\mathrm{O}\otimes[\nu(sd)^3]$-structure, is characterised by (3p-0h) states with even parity. Another possibility is a (2p-2h) proton excitation of the ^{16}O-core, this corresponds to the (5p-2h) states with the $^{14}\mathrm{C}\otimes[\pi(sd)^2\otimes\nu(sd)^3]$-structure. The configurations have a strong parentage to the ($^{14}\mathrm{C}\otimes\alpha$)-cluster configuration. Further we may expect the molecular ($^{12}\mathrm{C}\otimes 3n\otimes\alpha$)-structure consisting of a ^{12}C-core and an α-particle, bound by valence neutrons. In a shell model description this corresponds to a (7p-4h) configuration with 2 protons and 5 neutrons in the (sd) shell corresponding to a $^{12}\mathrm{C}\otimes[\pi(p)^2\otimes\nu(p)^2]_\alpha\otimes\nu(sd)^3$-structure. An odd-particle–odd-hole excitation produces odd-parity states by excitation from the ($1p$) shell to the (sd) shell. However, the rotational bands of negative parity are more difficult to identify in the present study —they represent the parity inversion partners. For ^{19}O the cluster bands (the $K^\pi = 3/2^+$ and $3/2^-$ bands) will appear in the shell model as (5p-2h, 6p-3h), the maximum spin of the positive-parity band is expected as $17/2^+$.

At even higher excitation energies states with *oblate* shapes are expected. Four α-particles may be, for example, placed in a plane with three covalent neutrons shared by all four α-particles. A similar configuration has been identified as the triangular shapes in ^{14}C both experimentally and in calculations [31,32,34,35].

3.1 Bansal-French-Zamick weak-coupling calculations

Properties of the excited states of nuclei whose configurations consist of holes in the $1p$-shell and particles in the $2s1d$-shell can be studied in a weak-coupling scheme following the idea of Bansal and French [36] and Zamick (BFZ) [37]. To estimate the position of the mp-nh states, one can use the following relation for the excitation energy $E_x(m\text{p-}n\text{h})$:

$$E_x(m\text{p-}n\text{h}) = M(m\text{p}) + M(n\text{h}) + amn + \frac{1}{2}b[T(T+1) - T_p(T_p+1) - T_h(T_h+1)] - cm_\pi n_\pi, \quad (1)$$

where m_π and n_π denote the number of proton particles and holes, respectively; T_p is the isotopic spin of m-particles, T_h is the isotopic spin of n-holes and the entire nucleus has isotopic spin T. Here $M(m\text{p})$ and $M(n\text{h})$ represent the masses of nuclei obtained relative to cores with (0p, 0h); for example: for the 5p-2h states, using $m=5$, $n=2$, $T=3/2$, $T_p=1/2$, $T_h=1$, $m_\pi=n_\pi=2$, one gets

$$E_x(5\text{p-}2\text{h}) = M(^{21}\mathrm{Ne}) + M(^{14}\mathrm{C}) - M(^{19}\mathrm{O}) + 10a + 1/2b - 4c. \quad (2)$$

With standard parameters [38,39] for this mass region ($a=0.41$ MeV, $b=4.9$ MeV and $c=0.34$ MeV) one gets $E_x(5\text{p-}2\text{h}) = 3.88$ MeV for ^{19}O. Since α-cluster states are in the shell model described as superpositions of different multi-particle–multi-hole configurations, BFZ calculations usually position them too high in excitation energy (*e.g.* the 0_2^+ state in ^{16}O is calculated ≈ 1 MeV too high). Therefore, the actual excitation energy of the first α-cluster state (band-head of the rotational band) in ^{19}O should be expected at around $E_x \approx 3.0$ MeV. The simple OXBASH calculations for ^{19}O [21] also predict this state at a bit higher excitation energy.

For the 4p-1h states (with proton hole), the band discussed in sect. 4.3, using $m=4$, $n=1$, $T=3/2$, $T_p=1$, $T_h=1/2$, $m_\pi=n_\pi=1$ one finds

$$E_x(4\text{p-}1\text{h}) = M(^{20}\mathrm{F}) + M(^{15}\mathrm{N}) - M(^{19}\mathrm{O}) + 4a + 1/2b - c. \quad (3)$$

Table 2. Proposed members of the positive-parity $K^\pi = 3/2^+$ cluster band in ^{19}O. The following entries are shown: spins and parities J^π, excitation energies E_x, widths of resonances Γ and cross-sections $\mathrm{d}\sigma/\mathrm{d}\Omega$ (the extra parenthesis is given for uncertainties caused by overlapping, or unresolved states), cross-sections divided by $(2J+1)$. Parenthesis around cross-sections indicate increased uncertainties due to overlapping states (see text and figures).

J^π	E_x [MeV]	Γ [keV]	$(\mathrm{d}\sigma/\mathrm{d}\Omega)_{cm}$ [μb/sr] $(\mathrm{d}\sigma/\mathrm{d}\Omega)/(2j+1)$ $\theta_{lab} = 10^\circ$	$(\mathrm{d}\sigma/\mathrm{d}\Omega)_{cm}$ [μb/sr] $(\mathrm{d}\sigma/\mathrm{d}\Omega)/(2j+1)$ $\theta_{lab} = 20^\circ$	$(\mathrm{d}\sigma/\mathrm{d}\Omega)_{cm}$ [μb/sr] $(\mathrm{d}\sigma/\mathrm{d}\Omega)/(2j+1)$ $\theta_{lab} = 39^\circ$
$3/2^+$	3.066(4)		0.47(5)	0.25(4)	0.16(2)
			0.12	0.06	0.04
$(5/2)^+$	4.327(5)	5	0.89(7)	0.79(7)	0.37(4)
			0.15	0.13	0.06
$(7/2)^+$	5.502(3)	13	1.79(13)	1.18(8)	0.72(5)
			0.22	0.15	0.09
$(9/2)^+$	7.128(4)	13	4.28(13)	4.27(14)	1.97(8)
			0.43	0.43	0.20
$(11/2)^+$	9.251(5)	15	7.82(18)	7.23(19)	3.87(10)
			0.65	0.60	0.32
$(13/2)^+$	12.038(5)	15	8.52(17)	(13.81(32))	2.55(9)
			0.61	0.99	0.18
$(15/2)^+$	14.956(6)	110	8.86(19)	13.24(29)	5.99(12)
			0.54	0.83	0.37
$(17/2)^+$	18.074(13)	109	(18.65(29))	(9.71(27))	7.26(15)
			1.04	0.52	0.40

Using the same parameters as above, we get for the first state, E_x(4p-1h) = 5.24 MeV. Since such states are not cluster states, BFZ calculations should give a rather good estimate of their position. Similar calculations for the ^{18}O case predict positions of the α-cluster and proton-hole band-heads [6] with rather high accuracy.

4 Results for rotational bands in ^{19}O

The excitation energy, E_x, of the members of a rotational band depends on the total angular momentum J as follows [40]:

$$E_J = \frac{\hbar^2}{2\Theta}\,[J(J+1)] + E_0. \qquad (4)$$

Here Θ is the moment of inertia of the deformed nucleus in a given configuration and E_0 is the band-head energy. We present here results for two proposed parity split bands.

In order to be able to propose bands in the present work, where very little is known on the spins (and our assignments based on the yields being proportional to $2J+1$ are only provisional), we use several points:
i) in view of the bands established for ^{18}O: *we use the weak-coupling model for the additional neutron*,
ii) the band-head for the positive-parity $K = 3/2^+$ band is expected close to the $K = 0_2$ band in ^{18}O;
iii) the relation between E_x and J; according to the weak-coupling model we will place the band parallel to the $K = 0_2$ band in ^{18}O "starting" with the 17/2 spin value for the strong peak at 18.07 MeV with a width of 109 keV;
iv) information from the $(2J+1)$-dependence of cross-sections and their angular dependences.

The parity splitting should also be similar to the parity doublet $K = 0_2^{+,-}$ bands in ^{18}O, (*i.e.* ~ 4.0 MeV). Thus all proposed bands in ^{19}O will have very similar structure to those established in ^{18}O (weak-coupling model) for the extra valence neutron. The rotational bands proposed in this way are shown in tables 2, 3 and 4, and in figs. 6 and 7.

4.1 Parity splitting of rotational cluster bands

The cluster and molecular structures studied in the oxygen isotopes of the present work consist of two different species, *i.e.* of two clusters of different size (for example $^{14}\mathrm{C}\otimes\alpha$). Such cluster structures usually correspond to octupole deformations of the nucleus, which implies intrinsic reflection asymmetry and rotational bands as parity inversion doublets, as already described in ref. [6]. From the linear combinations of two reflected states, using a positive and a negative sign, respectively, we obtain a splitting of the rotational bands into two parities. The feature of symmetry breaking has been explored in nuclear physics by Bohr and Mottelson [40], where this phenomenon appears with the odd multipoles of deformation, in particular with the octupole deformation [40–42]. The energy

Table 3. As table 2: proposed members of the negative-parity, $K^\pi = 3/2^-$, cluster band in ^{19}O. The following entries are shown: spins and parities J^π, excitation energies E_x, widths of resonances Γ and cross-sections $\mathrm{d}\sigma/\mathrm{d}\Omega$, cross-sections divided by $(2J+1)$.

J^π	E_x [MeV]	Γ [keV]	$(\mathrm{d}\sigma/\mathrm{d}\Omega)_{cm}$ [μb/sr] $(\mathrm{d}\sigma/\mathrm{d}\Omega)/(2j+1)$ $\theta_{lab} = 10^\circ$	$(\mathrm{d}\sigma/\mathrm{d}\Omega)_{cm}$ [μb/sr] $(\mathrm{d}\sigma/\mathrm{d}\Omega)/(2j+1)$ $\theta_{lab} = 20^\circ$	$(\mathrm{d}\sigma/\mathrm{d}\Omega)_{cm}$ [μb/sr] $(\mathrm{d}\sigma/\mathrm{d}\Omega)/(2j+1)$ $\theta_{lab} = 39^\circ$
$(3/2^-)$	6.970(5)	26	1.91(7)	1.78(9)	0.82(5)
			0.48	0.45	0.21
$(5/2)^-$	7.602(4)	7	2.96(11)	2.90(12)	1.72(8)
			0.49	0.48	0.29
$(7/2)^-$	9.055(5)	37	4.21(13)	4.27(14)	1.66(7)
			0.52	0.53	0.21
$(9/2)^-$	10.152(5)	60	4.33(14)	6.22(17)	2.25(9)
			0.43	0.62	0.23
$(11/2)^-$	13.103(4)	220	9.50(18)	9.40(27)	5.34(12)
			0.79	0.78	0.45
$(13/2)^-$	15.483(35)	320	(24.26(31))	(18.04(34))	
			1.73	1.29	
$(15/2)^-$	18.300(9)	290	(20.96(31))		
			1.31		
$(17/2)^-$	19.705(18)	230	(20.48(51))		
			1.14		

Table 4. As table 3: proposed members of the negative-parity $K^\pi = 3/2^-$ band in ^{19}O of shell model states with a proton-hole configuration. The following entries are shown: spins and parities J^π, excitation energies E_x, widths of resonances Γ and cross-sections $\mathrm{d}\sigma/\mathrm{d}\Omega$, cross-sections divided by $(2J+1)$.

J^π	E_x [MeV]	Γ [keV]	$(\mathrm{d}\sigma/\mathrm{d}\Omega)_{cm}$ [μb/sr] $(\mathrm{d}\sigma/\mathrm{d}\Omega)/(2j+1)$ $\theta_{lab} = 10^\circ$	$(\mathrm{d}\sigma/\mathrm{d}\Omega)_{cm}$ [μb/sr] $(\mathrm{d}\sigma/\mathrm{d}\Omega)/(2j+1)$ $\theta_{lab} = 20^\circ$	$(\mathrm{d}\sigma/\mathrm{d}\Omega)_{cm}$ [μb/sr] $(\mathrm{d}\sigma/\mathrm{d}\Omega)/(2j+1)$ $\theta_{lab} = 39^\circ$
$(3/2^-)$	5.362(4)	13	1.28(9)	1.27(8)	0.79(5)
			0.32	0.32	0.20
$(5/2)^-$	7.504(6)	4	3.65(11)	2.580(12)	1.61(8)
			0.55	0.43	0.26
$(7/2)^-$	10.351(5)	7	2.90(10)	5.16(19)	3.05(10)
			0.36	0.65	0.38
$(9/2)^-$	13.243(7)	22	2.54(10)	2.95(15)	3.83(10)
			0.25	0.30	0.38
$(11/2)^-$	17.290(5)	9	(10.20(26))	(9.64(24))	(8.30(17))
			0.85	0.80	0.69

splitting, E^+-E^-, is equal to $2\cdot\delta_E$ (see ref. [6]). The value of this energy splitting reflects the intrinsic structure, for completely rigid clusters it will be zero. We expect for the $K = 3/2$ doublet in ^{19}O a splitting similar to ^{18}O ($K = 0_2$), also the moments of inertia are expected to be very similar.

4.2 The $K^\pi = 3/2^+$ cluster band

Some low-lying members of this band are known from the literature, the energy dependence is chosen to be close to the ^{18}O ($K = 0_2$) band. The differential cross-sections are summarised in the tables. For the proposed members of rotational bands the dependence on the statistical fac-

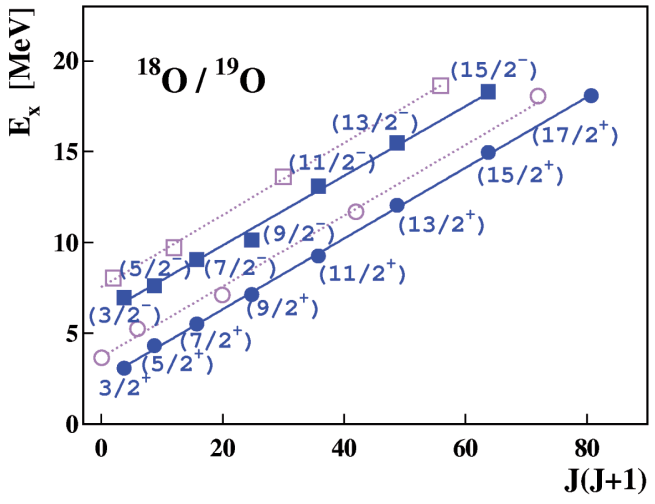

Fig. 6. (Color online) Proposed energy systematics for the members of the ^{19}O rotational bands (blue, full symbols) forming the parity inversion doublet with $K^\pi = 3/2^\pm$, as a function of $J(J+1)$. In parallel we have plotted the bands with $K^\pi = 0_2^\pm$ in ^{18}O (open symbols), see also tables 2, and 3.

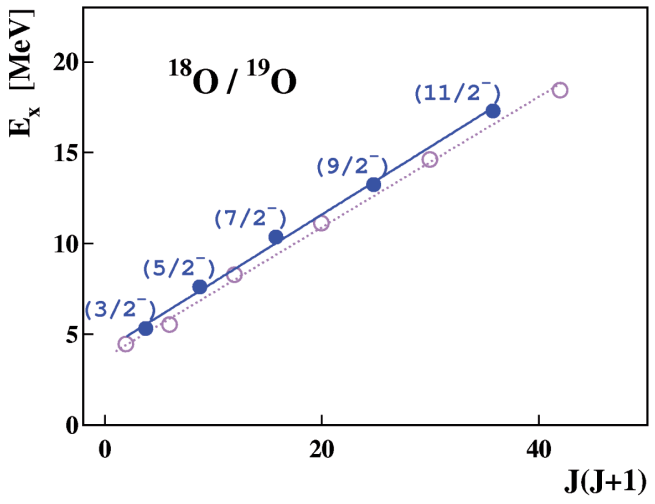

Fig. 7. (Color online) Proposed energies of the members of the $K = 3/2^-$ one-proton excitation band in ^{19}O as a function of $J(J+1)$. A comparison is given with the analog band in ^{18}O (open symbols).

tor $(2J+1)$ is tested, the relevant numbers for the ratios are given in table 2 (see also fig. 6). Some comments are needed because of the increasing values of these ratios with larger spins and some individual larger cross-sections, these are mostly caused by unresolved states close by. The corresponding cross-sections are placed in brackets, unresolved states usually cause a too large cross-section for the state assumed.

The highest spins often show a larger value of the ratio $(\mathrm{d}\sigma/\mathrm{d}\Omega)/(2J+1)$, this can be due to the direct reactions, which are expected to contribute more to states with higher spins. In addition in many nuclei a simultaneous increase in the spectroscopic factors for α-particles with increasing spin and excitation energy is observed. Another problem is connected to the matching conditions between the incoming and outgoing particles, in the region of high-spin states the gap can be bridged more easily. Both effects can explain the deviations from the $(2J+1)$ phase-space rule, in particular for the low-lying low-spin states. In the case of negative-parity partners (table 3), placed at higher excitation energies, the deviations are less pronounced, in particular if the average over all three angles are considered. Actually in some regions of excitation energies above 10 MeV, the separation of broader states is not unique, in the relevant tables some cross-section are thus placed in parenthesis.

4.3 $K^\pi = 3/2^-$ cluster band

In order to establish the inversion partner with negative parity (see fig. 6), we use several guidelines for its identification: strong population, larger widths (as compared to the positive-parity band) and the energy splitting $2 \cdot \delta_E$. In the weak-coupling model we expect the energy splitting for the cluster parity doublet in ^{19}O to be similar to the one in ^{18}O (4.0 MeV, it could also be slightly smaller) and therefore a $3/2^-$ band-head for the negative-parity cluster band close to 7.0 MeV is proposed. We have localised states which we tentatively place into a rotational band ending with a 17/2 state at 19.7 MeV (see table 3). Concerning the phase-space factor $(2J+1)$ the same arguments as for the positive-parity band apply, in addition we may point to the fact that the rule actually has to be applied to the integrated cross-sections and the higher spins have a smaller decrease with angle. Concerning the width, we use the observation in many of theoretical calculations for many cluster bands that the negative-parity bands show more pronounced clustering [2], and that they have a larger cluster width, which is expressed in a larger width in keV, and in an increasing cross-section with excitation energy.

We should also cite here, that the shell model calculations for ^{18}O in ref. [6] cannot reproduce the members of the negative-parity band, because they correspond to excitations into the fp-shell. There the GCM calculations by Descouvemont and Baye [43] as well as the (AMD + GCM) calculations by Furutachi *et al.* in refs. [26,27] are shown to reproduce very well the members of the $K^\pi = 0_2^-$ negative-parity partner of the inversion doublet. The situation is very similar to the case of ^{21}Ne [4,9], with the same number (3) of valence neutrons, there the parity (energy) splitting between the two $K^\pi = 3/2\pm$ bands is ~ 4.0 MeV, which is very close to the value in ^{20}Ne.

4.4 Shell-model–like $K^\pi = 3/2^-$ band

In addition to the ground-state band, the cluster inversion doublet bands described above, a negative-parity configuration band with a one-proton excitation based

on the 4.457 MeV ($J^\pi = 1^-_1$) state have been found in ^{18}O. For ^{19}O the first three members $J^\pi = 3/2^-, 5/2^-$ and $7/2^-$ of this $K^\pi = 3/2^-$ band are known states with a well-established spin assignment [10]. In order to identify higher-lying members for possible candidates, we have examined the systematics of excitation energies in dependence on $J(J+1)$ by extrapolating the trend to $J = 9/2$, $J = 11/2$ and $J = 13/2$. Furthermore, we took into account that all states in this band are very narrow (< 30 keV) and have a large cross-section, see, *e.g.*, fig. 4. The ratios of the cross-sections with phase space give good agreement (in particular at 39° degrees), except for the last narrow state —this state appears to be strong; it is probably an yrast state and as such it is particularly well matched. Inspecting the spectra we again emphasise that the yields are subject to uncertainties, because of the potential overlap with other (broader) states.

5 Survey of states

In this section we discuss shortly the observed states, a complete spectroscopy does not seem to be possible for the present case. Spin determinations with angular-correlation experiments for states emitting α-particles would be necessary. Some restrictions on spins have been obtained from β-decay studies, these are entered in the final tables with the indication (β, γ). In the present experiment we have observed in total 109 states (50 are new) up to an excitation energy of 20 MeV. The reaction may still be selective in the population and the resolution of 45 keV implies that above 10 MeV of excitation energy we may have missed a considerable number of states due to overlaps in energy. With the described methods we have attempted to place the dominantly populated states into rotational bands, which correspond to i) shell model configurations, ii) parity inversion doublets, cluster bands and iii) molecular bands. For further use we give in the appendix the complete list of all observed states.

Although the expected simplicity of the structure of ^{19}O makes it an appealing nucleus to investigate, it is rather difficult to study this nucleus experimentally. Spectroscopy of ^{19}O has been made mainly by the ^{18}O(n,n) [44], ^{18}O(d,p) [45], ^{17}O(t,p) [46–48], and ^{13}C(^{7}Li$,p$) [49–51] reactions. Angular correlations for the ^{18}O(d,p) reaction are consistent with $J^\pi = 5/2^+$ for the ground state and unambiguously fix $J^\pi = 3/2^+$ and $1/2^+$, respectively, for the ^{19}O*(0.096, 1.47 MeV). A lot of spectroscopic information was obtained from the measurement of the ^{18}O(d,p) reaction at $E_d = 15$ MeV [52]. The ^{18}O$(\alpha, ^3$He) reaction has also been investigated [53]. Most of the spin assignments has been derived from the total cross-sections and $2J+1$ analysis for the ^{13}C(^{7}Li$,p$) reaction at $E(^7\text{Li}) = 16$ MeV [51].

5.1 Shell model states

Detailed spectroscopic information of the ^{19}O nucleus is given in ref. [48]. The ground state definitely has the simple $(d_{5/2}s_{1/2})^3$ configuration [46], as well as the first four excited states (up to the $7/2^+$ state at $E_x = 2.779$ MeV). Shell model counter-partners were clearly identified [48] for the ground state and the states at $E_x = 0.10$, 1.47, 2.37, 2.78, 3.07 and 5.46 MeV, while the strong but less definite correspondence exists for the states at $E_x = 3.16$, 4.11, 4.71, 5.00, 5.15 and 5.50 MeV. As claimed by the authors [48], the remaining low-lying states, those at $E_x = 3.23$, 3.95, 4.33, 4.40, 4.58, 5.53, 5.71, 6.13, 6.20 and 6.28 MeV, do not appear to have $(sd)^3$ configurations.

From weak-coupling considerations and calculations in a truncated shell model space, it is expected [14] that the lowest-lying $\geq 2\hbar\omega$ intruder state in ^{19}O lie at 3–4 MeV and has $J^\pi = 3/2^+$. This state is identified as the 3067 keV state, contrary to the results of Crozier *et al.* [48]. Shell model calculations in ref. [24] identify the first 5p-2h state as the one at $E_x = 3.067$ MeV (which agrees with the result in ref. [14]), while the second one is calculated at $E_x = 4.82$ MeV and no correspondence to the experimentally known state is suggested.

It is interesting to note that the state at $E_x = 3.945$ MeV ($J^\pi = 3/2^-$) is bound by only 15 keV so it is suggested to have a halo structure. There are $\approx$ 40 more known states up to $E_x = 11.58$ MeV [10], most of them seen only in the ^{13}C(^{7}Li,p) reaction [12]. The two highest listed states in this compilation ($E_x = 11.25$ and 11.58 MeV) are seen only as resonances in the excitation function of the ^{18}O(n,α) reaction.

$E_x = 5.362$ MeV, $J^\pi = (3/2^-)$

The first state of the shell-model–like $K = 3/2^-$ band is the one at $E_x = 5.362$ MeV (the excitation energy listed in the last compilation [10] is 5.384 MeV, while the spin assigned to it is $9/2 \rightarrow 13/2$). Prior to this work, this state has been seen only in the ^{13}C(^{7}Li$,p$) reaction [12], where its high spin has been suggested.

5.2 Rotational bands, cluster states

Here we review the existing spectroscopic information of states belonging to the rotational bands. Since the experimental data for ^{19}O is still rather scarce, these information are given only for the lowest-lying states.

$E_x = 3.066$ MeV, $J^\pi = (3/2^+)$

The state at $E_x = 3.066$ MeV (in compilation tentatively assigned $J^\pi = 3/2^+$) is suggested to be the lowest-lying $\geq 2\hbar\omega$ intruder state in ^{19}O [14]; see the detailed discussion in the appendix of ref. [14]. This contradicts the claim that the state at $E_x = 3.232$ MeV is a 5p-2h core-excited state [48], which would require $J^\pi = 3/2^+$, while in the compilation it is listed to have $J^\pi = (1/2, 3/2)^-$. In any case, one of these two states is the band-head of

the $3/2^+$ cluster rotational band, probably the one at $E_x = 3.066\,\text{MeV}$. This is also supported by the recent result [15] that the 3.232 MeV state is populated by the β-decay of ^{19}N, which would imply spin/parity $J^\pi = 1/2^-$ or $3/2^-$. Shell model calculations in ref. [24] also identify the first 5p-2h state as the one at $E_x = 3.066\,\text{MeV}$.

$E_x = 4.327\,\text{MeV},\ J^\pi = (5/2^+)$

This state has been seen in different complicated reactions, like the $^{13}\text{C}(^7\text{Li}, p)$ reaction [12]. On the other hand, it has no measurable strength in the $^{17}\text{O}(t, p)$ reaction at 12 MeV [47,48], indicating that its structure is not shell-model-like. Shell model calculations in ref. [24] finds the second 5p-2h state at $E_x = 4.82\,\text{MeV}$ (no corresponding experimentally known state is suggested).

$E_x = 5.502\,\text{MeV},\ J^\pi = (7/2^+)$

This state has been seen in a number of different reactions, like $^{13}\text{C}(^7\text{Li}, p)$, $^{17}\text{O}(t, p)$ and $^{18}\text{O}(d, p)$. It was rather strongly populated in the $^{18}\text{O}(d, p)$ reaction at 15 MeV [52]. In the early systematics of the ^{19}O states [48], it is suggested to be dominantly the $d_{3/2}$ single-particle state.

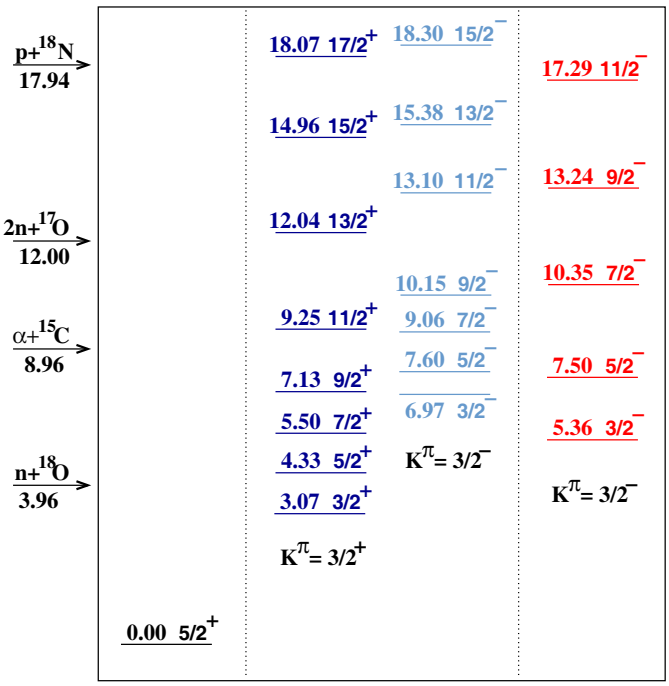

Fig. 8. (Color online) Proposed level diagrams for all bands discussed for ^{19}O. Spins and parities of all states in tables are those suggested in this work (except for the ground and the 3.07 MeV state which were taken from ref. [10]). Middle column: rotational bands based on the $^{14}\text{C} \otimes n \otimes \alpha$ configuration. Right column: band based on the shell model configuration with a proton hole.

6 Conclusions

We conclude that the used multi-nucleon transfer reaction was an excellent choice to observe many new states in ^{19}O up to high excitation energy. Although spin assignments were not possible directly, we were able to use cross-section and energy systematics to establish the lowest-lying parity inversion bands. The weak-coupling model has been applied to establish bands in close correspondence to those in ^{18}O. These are most likely due to the neutron in π-molecular orbitals, similar to the equivalent case in ^{21}Ne [4].

The final table shown in the appendix shows all observed states (not necessary complete because of overlapping broad levels). Many states at higher excitation have not been assigned. Among these are still a large number of shell model states, but actually we expect, similar to the case of ^{21}Ne, bands with σ binding for the valence neutron in the $(^{14}\text{C} \otimes 1n \otimes \alpha)$ configuration. These are well above the threshold for neutron emission and are expected to be broad states. In addition a parity inversion doublet as in ^{18}O, based on the $(^{12}\text{C} \otimes 3n \otimes \alpha)$ configuration can be expected —these states are all well above 10 MeV excitation energy and should have a larger width. In the final table we have listed some cases where unresolved states are known, however, we must expect many more of these. So the "complete" spectroscopy of ^{19}O appears very difficult (potentially impossible).

In fig. 8 we give an overview of the proposed bands in ^{19}O, the moments Θ of inertia (given as $\hbar^2/2\Theta$) of the parity doublets bands are given. The moments of inertia of those bands are large and correspond to distinctly large deformations due to the cluster structure suggested in fig. 1. The present study of bands in isotopes of oxygen [27,6,7], ^{18,19,20}O, clearly suggests, that the parity inversion doublets can be observed as predicted by the cluster structure: namely the $(^{14}\text{C} \otimes {}^6\text{He})$-structure and the $(^{14}\text{C} \otimes \text{X}n \otimes \alpha)$ molecular structures with covalent binding by the neutron.

The technical staff at MLL is gratefully acknowledged for the stable operation of the accelerator with the high-current ^{7}Li-beam.

Appendix A. Table of all observed states

We give here in table 5 a complete list of all states observed. This list could serve in future work in order to establish a more complete spectroscopy of ^{19}O. Our bands are numbered Bd_i and some states have restricted spin values due to experimental studies using (β, γ)-coincidences.

Table 5. List of all states in ^{19}O observed in the present work. The proposed members of the bands are marked in the first column by $Bd_{1,2}$ for the parity inversion doublet with $K^\pi = 3/2$, and as Bd_3 for the 1 proton-hole band. For some cases additional states from the literature are given with their experimental source (*e.g.* β, γ). The following entries are shown: excitation energies E_x, widths of resonances Γ and cross-sections $\mathrm{d}\sigma/\mathrm{d}\Omega$ at three angles, spins and parities J^π from the literature or our assignment in parenthesis. Some of the shell model configurations are also indicated in the first column.

Conf.	E_x [MeV]	Γ [keV]	$(\frac{\mathrm{d}\sigma}{\mathrm{d}\Omega})_{cm}$ [μb/sr] $\theta_{lab} = 10°$	$(\frac{\mathrm{d}\sigma}{\mathrm{d}\Omega})_{cm}$ [μb/sr] $\theta_{lab} = 20°$	$(\frac{\mathrm{d}\sigma}{\mathrm{d}\Omega})_{cm}$ [μb/sr] $\theta_{lab} = 39°$	J^π_{Lit} (new)	E_{Lit} [MeV]	Γ_{Lit} [keV]
$(sd)^3$	0.000(3)		0.80(10)	0.69(6)	0.19(3)	$5/2^+$	0.000	
$(sd)^3$	0.098(4)		0.77(10)	0.39(5)	0.22(3)	$3/2^+$	0.096	
$(sd)^3$	1.471(4)		0.24(5)	0.26(4)	0.12(2)	$1/2^+$	1.472	
$(sd)^3$	2.374(4)		0.91(10)	0.11(3)	0.64(5)	$9/2^+$	2.372	
$(sd)^3$	2.775(3)		1.44(13)	0.92(7)	0.51(4)	$7/2^+$	2.779	
Bd_1	3.066(4)		0.47(5)	0.25(4)	0.16(2)	$(3/2)^+$	3.067	
$(sd)^3$	3.154(4)		0.86(7)	0.86(7)	0.28(3)	$5/2^+$	3.154	
$(sd)^3$	3.227(4)		0.84(7)	0.62(6)	0.47(4)	$(3/2^+)$	3.237	
$(sd)^3$						$(1/2^-)$	3.232	β, γ
$(sd)^3$	3.946(3)		4.14(16)	2.88(13)	1.40(7)	$3/2^-$	3.945	β, γ
$(sd)^3$						$7/2^+$	3.949	
$(sd)^3$	4.106(4)	7	0.63(6)	0.52(5)	0.23(3)	$3/2^+$	4.1025	< 15
Bd_1	4.327(5)	5	0.89(7)	0.79(7)	0.37(4)	$(5/2^+)$	4.328	< 15
						1/2-,3/2-	4.434	β, γ
	4.404(5)	13	0.76(7)	0.82(7)	0.32(3)	3/2,5/2,7/2	4.403	< 15
	4.594(4)	42	1.56(10)	1.45(9)	0.47(4)	$3/2^-$	4.582	52
	4.703(5)	7	1.32(9)	1.16(8)	0.78(5)	$5/2^+$	4.703	< 15
	4.943(5)	4	0.60(6)	0.62(6)	0.29(3)	5/2,7/2	4.968	
	4.994(5)	11	1.51(9)	1.32(8)	0.73(5)	3/2,5/2	5.007	< 15
	5.073(5)	13	0.29(4)	0.16(3)	0.05(1)	$1/2^-$	5.082	49
	5.151(4)	19	0.89(7)	0.88(7)	0.29(3)	$5/2^+$	5.148	3
Bd_3	5.362(4)	13	1.28(9)	1.27(8)	0.79(5)	$(3/2^-)$	5.384	
Bd_1	5.502(3)	13	1.79(10)	1.18(8)	0.72(5)	$(7/2^+)$	5.504	< 15
	5.573(5)	10	0.22(4)	0.09(2)		$3/2^+$	5.54	490
	5.698(5)	22	0.41(4)	0.44(5)	0.21(3)	$5/2, 7/2^-$	5.705	8
	6.116(4)	13	2.22(9)	1.48(8)	0.88(5)	$3/2^+$	6.120	110
							6.192	
	6.261(6)	17	0.33(4)	0.67(6)	0.40(4)	$7/2^-$	6.269	19
	6.398(3)	10	1.14(7)	1.43(8)	0.76(5)		6.406	
	6.463(7)	12	0.62(5)	0.81(6)	0.65(5)	7/2,9/2,11/2	6.466	
	6.590(4)	18	5.41(15)	5.73(17)	1.96(8)		6.583	
	6.671(6)	20	0.47(4)	0.47(5)	0.70(5)			
	6.774(6)	32	0.38(4)	0.69(6)	0.38(4)			
	6.887(6)	10	0.35(4)	0.25(3)	0.19(3)		6.903	
Bd_2	6.970(5)	26	1.91(9)	1.78(9)	0.82(5)	$(3/2^-)$	6.988	
						$(1/2, 3/2^-)$	7.053	β, γ
Bd_1	7.128(4)	13	4.28(13)	4.27(14)	1.97(8)	$(9/2^+)$	7.118	
	7.235(5)	39	0.34(4)	3.57(13)	1.98(8)		7.242	
Bd_3	7.504(6)	4	3.65(12)	2.58(11)	1.61(7)	$(5/2^-)$	7.508	
Bd_2	7.602(6)	4	2.96(11)	2.90(12)	1.72(8)	$(5/2^-)$		
	7.826(6)	15	0.43(4)	0.21(3)	0.25(3)			
	8.055(5)	12	1.33(7)	1.20(8)	0.47(3)		8.048	
	8.118(5)	30	0.54(5)	0.60(5)	0.46(3)		8.132	
	8.189(5)	28	0.70(5)	0.73(6)	0.45(3)			
							8.247	
	8.411(5)	20	1.62(8)	1.63(9)	0.66(4)		8.450	
	8.537(7)	82	2.18(10)	2.13(10)	1.80(7)		8.561	
						$(1/2, 3/2^-)$	8.743	β, γ
	8.748(6)	70	2.85(11)	3.13(12)	1.57(6)			
	8.865(6)	53	1.14(7)	1.59(9)	1.09(5)		8.916	
							8.923	

Table 5. Continued.

J^π	E_x [MeV]	Γ [keV]	$(\frac{d\sigma}{d\Omega})_{cm}$ [μb/sr] $\theta_{lab} = 10^\circ$	$(\frac{d\sigma}{d\Omega})_{cm}$ [μb/sr] $\theta_{lab} = 20^\circ$	$(\frac{d\sigma}{d\Omega})_{cm}$ [μb/sr] $\theta_{lab} = 39^\circ$	J^π_{Lit} (new)	E_{Lit} [MeV]	Γ_{Lit} [keV]
	8.983(6)	53	1.86(9)	2.16(10)	1.42(6)			
							9.022	
Bd_2	9.055(5)	37	4.21(13)	4.27(14)	1.66(7)	$(7/2^-)$	9.064	
Bd_1	9.251(5)	15	7.82(18)	7.23(19)	3.87(10)	$(11/2^+)$	9.253	
							9.324	
	9.416(7)	15		0.58(5)			9.43	
	9.494(5)	83	2.22(10)	3.40(13)	0.24(2)			
							9.56	
	9.619(7)	78	1.07(7)	1.31(8)	2.15(7)	$7/2^-$	6.6	
	9.712(5)	12	1.53(8)	1.91(10)	1.56(6)			
	9.810(9)	25	0.99(7)	0.78(6)	0.33(3)			
						$7/2^-$	9.9	
	9.941(6)	58	2.63(11)	2.64(11)	1.96(8)		9.93	
	10.003(6)	14	1.13(7)	0.89(7)			9.98	
	10.086(7)	32	1.77(9)	1.20(8)	0.74(5)			
Bd_2	10.152(5)	60	4.33(14)	6.22(17)	2.25(9)	$(9/2^-)$		
						$7/2^-$	10.21	
	10.351(5)	7	2.90(10)	5.16(19)	3.05(10)			
						$1/2, 3/2^-$	10.573	β, γ
	10.660(5)	19	1.10(6)	2.39(13)	2.25(9)	$7/2^-$	10.66	
	10.792(5)	15			0.46(4)			
	10.920(20)	167	11.12(19)	9.80(27)	5.76(14)			
	11.248(11)	87		3.97(17)	2.63(9)		11.25	240
	11.587(5)	52	1.08(6)	1.51(10)	2.62(9)		11.58	330
	11.693(5)	20	2.58(9)	3.94(17)	1.94(6)			
	11.771(5)	17	1.91(8)	2.96(15)	1.65(7)			
	11.848(5)	143	4.50(12)	5.99(21)	1.53(7)			
Bd_1	12.038(5)	5	8.52(17)	13.81(32)	2.55(9)	$(13/2^+)$		
	12.055(13)	200	5.02(13)	4.05(17)	3.41(11)			
	12.235(5)	34	2.20(8)	2.11(13)	1.15(6)			
	12.328(6)	32	1.93(8)	1.68(11)	1.14(6)			
	12.429(6)	102	3.84(12)	3.60(17)	3.66(10)			
	12.557(7)	38	1.91(9)	1.04(9)	1.17(6)			
	12.649(8)	35	1.42(7)					
	12.702(8)	50		1.12(9)	1.08(5)			
	12.804(11)	118	5.21(14)	4.05(18)	4.04(10)			
Bd_2	13.103(15)	220	9.50(19)	9.40(27)	5.34(12)	$(11/2^-)$		
Bd_3	13.243(7)	22	2.54(10)	2.95(15)	3.83(10)	$(9/2^-)$		
	13.444(9)	103	4.07(13)	3.71(17)	3.61(10)			
	13.715(9)	20		0.99(9)	0.36(3)			
	13.860(5)	22	3.70(12)	3.06(15)	1.62(7)			
	13.920(14)	153	7.99(18)	5.99(21)	3.61(10)			
	14.131(9)	60	2.44(10)	1.73(11)	1.03(5)			
	14.292(9)	52	1.16(7)	1.80(11)	1.07(5)			
	14.437(9)	87	2.71(10)	2.61(13)	1.98(7)			
	14.633(9)	90		3.01(14)	1.63(6)			
	14.799(12)	195	6.47(16)		2.47(8)			
	14.841(12)	180		2.89(14)				
Bd_1	14.956(6)	110	8.86(19)	13.24(29)	5.99(12)	$(15/2^+)$		
	15.091(6)	7	2.68(10)	2.32(12)	0.73(4)			
	15.293(7)	118	5.65(15)	8.15(23)	4.16(10)			
Bd_2	15.483(35)	320	24.26(31)	18.04(34)		$(13/2^-)$		
	15.501(6)	10	1.41(8)					
	15.671(6)	35	2.61(10)					

Table 5. Continued.

J^π	E_x [MeV]	Γ [keV]	$(\frac{d\sigma}{d\Omega})_{cm}$ [μb/sr] $\theta_{lab} = 10^\circ$	$(\frac{d\sigma}{d\Omega})_{cm}$ [μb/sr] $\theta_{lab} = 20^\circ$	$(\frac{d\sigma}{d\Omega})_{cm}$ [μb/sr] $\theta_{lab} = 39^\circ$	J^π_{Lit} (new)	E_{Lit} [MeV]	Γ_{Lit} [keV]
	16.135(11)	253	21.13(37)	10.48(26)	6.69(16)			
	16.507(18)	120	4.59(17)					
	16.711(17)	340	24.04(40)	19.91(35)	9.77(19)			
	17.120(15)	267	12.67(29)	16.86(32)	7.94(17)			
Bd_3	17.290(5)	9	10.20(26)	9.64(24)	8.30(17)	$(13/2^-)$		
	17.436(9)	210	8.48(23)	10.79(26)	5.79(13)			
	17.628(8)	70	3.39(12)					
	17.801(8)	100		2.83(14)	1.63(7)			
Bd_1	18.074(13)	109	18.65(29)	9.71(27)	7.26(15)	$(17/2^+)$		
Bd_2	18.300(9)	290	20.96(31)			$(15/2^-)$		
	18.407(9)	230		17.40(36)	8.22(16)			
	18.625(9)	140	10.38(22)					
	18.694(9)	120		6.03(21)	1.45(7)			
	18.873(8)	133	12.58(24)	6.31(22)	2.24(8)			
	19.127(10)	140	7.23(30)					
	19.300(10)	60	4.10(23)					
Bd_2	19.705(18)	230	20.48(51)			$(17/2^-)$		
	20.589(14)	80	5.93(27)					

References

1. H. Horiuchi, K. Ikeda, Prog. Theor. Phys. Jpn. **40**, 277 (1968).
2. W. von Oertzen, M. Freer, Y. Kanada-En'yo, Phys. Rep. **432**, 43 (2006).
3. W. von Oertzen, Z. Phys. A **357**, 355 (1997).
4. W. von Oertzen, Eur. Phys. J. A **11**, 403 (2001).
5. M. Milin *et al.*, Eur. Phys. J. A **41**, 335 (2009).
6. W. von Oertzen *et al.*, Eur. Phys. J. A **43**, 17 (2010).
7. W. von Oertzen, H.G. Bohlen, T. Dorsch *et al.*, in preparation.
8. T. Dorsch, PhD Thesis, Technical University München (2008).
9. C. Wheldon, Tz. Kokalova, W. von Oertzen *et al.*, Eur. Phys. J. A **26**, 321 (2005).
10. D.R. Tilley, H.R. Weller, C.M. Cheves, R.M. Chasteler, Nucl. Phys. A **595**, 1 (1995), and later additions **636** (2000).
11. T. Stammbach, S.E. Darden, P. Huber, I. Sick, Helv. Phys. Acta **40**, 915 (1967).
12. H.T. Fortune, H.G. Bingham, Nucl. Phys. A **432**, 197 (1977).
13. J.B. McGrory, B.H Wildenthal, Phys. Rev. C **7**, 974 (1973).
14. E.K. Warburton, Phys. Rev. C **38**, 935 (1988).
15. C.S. Sumithrarachchi, D.W. Anthony, P.A. Lofy, D.J. Morrissey, Phys. Rev. C **74**, 024322 (2006).
16. A. Volya, V. Zelevinsky, Phys. Rev. Lett. **94**, 052501 (2005).
17. A. Volya, V. Zelevinsky, Phys. Rev. C **74**, 064314 (2006).
18. M. Wiedeking *et al.*, Phys. Rev. C **77**, 054305 (2008).
19. Y. Nagai, M. Segawa, T. Ohsaki, H. Matsue, K. Muto, Phys. Rev. C **76**, 051301(R) (2007).
20. T. Ohsaki, M. Igashira, Y. Nagai, M. Segawa, K. Muto, Phys. Rev. C **77**, 051303(R) (2008).
21. H.G. Bohlen *et al.*, Eur. Phys. J. A **31**, 279 (2007).
22. W.D.M. Rae, A. Etchegoyen, B.A. Brown, *OXBASH, The Oxford - Buenos Aires - MSU shell model code*, Technical Report 524, Michigan State University Cyclotron Laboratory (1985).
23. H.G. Bohlen *et al.*, Phys. Rev. C **68**, 054606 (2003).
24. J. Meissner, H. Schatz, J. Görres, H. Herndl, M. Wiescher, H. Beer, F. Käppeler, Phys. Rev. C **53**, 459 (1996).
25. M.G. Pellegriti *et al.*, Phys. Lett. B **659**, 864 (2008).
26. N. Furutachi, *et al.*, arXiv:0706.0145v1 [nucl-th] (2007).
27. N. Furutachi, *et al.*, Prog. Theor. Phys. Jpn. **119**, 403 (2008).
28. M. Gai *et al.*, Phys. Rev. C **43**, 2127 (1991).
29. M. Gai *et al.*, Phys. Rev. C **45**, R2548 (1992).
30. K. Sato, M. Tanigaki, T. Onishi *et al.*, Nucl. Phys. A **654**, Suppl. 1, 735c (1999).
31. W. von Oertzen *et al.*, Eur. Phys. J. A **21**, 193 (2004).
32. N. Itagaki *et al.*, Phys. Rev. Lett. **92**, 142501 (2004).
33. H.G. Bohlen, *Code SPEC (Version F)*, HMI Berlin, private communication (2003).
34. M. Milin, W. von Oertzen, Eur. Phys. J. A **14**, 295 (2002).
35. M. Milin, W. von Oertzen, Fizika (Zagreb) B **12**, 61 (2003).
36. R. Bansal, J.B. French, Phys. Lett. **11**, 145 (1964).
37. L. Zamick, Phys. Lett. **19**, 580 (1965).
38. H.T. Fortune, J.N. Bishop, L.R. Medsker, B.H. Wildenthal, Phys. Rev. Lett. **41**, 527 (1978).
39. H.T. Fortune, R. Sherr, Phys. Rev. C **72**, 034304 (2005).
40. A. Bohr, B.R. Mottelson, *Nuclear Structure* Vol. **II** (World Scientific, 1998).
41. W. Nazarewicz *et al.*, Phys. Rev. Lett. **52**, 1272 (1984).
42. P.A. Butler, W. Nazarewicz, Rev. Mod. Phys. **68**, 350 (1996).
43. P. Descouvemont, D. Baye, Phys. Rev. C **31**, 2274 (1985).
44. P.E. Koehler, H.D. Knox, D.A. Resler, R.O. Lane, G.F. Auchampaugh, Nucl. Phys. A **453**, 429 (1986).
45. S. Sen, S.E. Darden, H.R. Hiddleston, W.A. Yoh, Nucl. Phys. A **219**, 429 (1974).
46. R. Moreh, Nucl. Phys. **70**, 293 (1965).

47. J.L. Wiza, R. Middleton, Phys. Rev. **143**, 676 (1966).
48. D.J. Crozier, H.T. Fortune, R. Middleton, J.L. Wiza, Phys. Rev. C **11**, 393 (1975).
49. J.L. Wiza, H.G. Bingham, H.T. Fortune, Phys. Rev. C **7**, 2175 (1973).
50. H.T. Fortune, H.G. Bingham, Phys. Rev. C **10**, 2174 (1974).
51. H.T. Fortune, H.G. Bingham, Nucl. Phys. A **293**, 197 (1977).
52. J.C. Armstrong, K.S. Quisenberry, Phys. Rev. **122**, 1508 (1961).
53. M. Yasue *et al.*, Phys. Rev. C **46**, 1242 (1992).